Astronomical & Astrophysical Transactions

The Journal of the Eurasian Astronomical Society

Heat- and radiative-driven implosion of interstellar clouds. i. initial dynamics

I. Kovalenko [a]; Yu. Shchekinov [b]
[a] University of Volgograd, Volgograd, USSR
[b] Institute of Physics, University of Rostov, Rostov on Don, USSR

PLEASE SCROLL DOWN FOR ARTICLE

HEAT- AND RADIATIVE-DRIVEN IMPLOSION OF INTERSTELLAR CLOUDS. I. INITIAL DYNAMICS

I. KOVALENKO[1] and YU. SHCHEKINOV[2]

[1] *University of Volgograd, 2nd Prodolnaya 20, Volgograd, 400062, USSR*
[2] *Institute of Physics, University of Rostov, Stachki 194, Rostov on Don, 344104, USSR*

The hydrodynamics of a spherical cloud, surrounded by hot intercloud gas or exposed by heating radiation, is investigated. Two principal types of hydrodynamical flows are shown to exist simultaneously: an outflow of gas from the outer layer of the cloud that corresponds to the cloud's evaporation, and cumulative compression of the cloud's interior. The cause of such flows is a pressure excess in the outer layers of the cloud created by heating of the cloud's gas by thermal conductivity or by radiation, which is assumed to be absorbed by the surface layers. The qualitative features of the dynamics of evaporating and compressing gas are described. In particular, an amplifying of the magnitude of compression of the cloud's interior in models with a dominating role of electronic conductivity and volume cooling is shown. The importance of these effects for the physics of interstellar matter is discussed.

KEY WORDS Interstellar matter, hydrodynamics

1. INTRODUCTION

One of the effects dominating the dynamics of multicomponent interstellar matter is mass and energy exchange at interface boundaries: the evaporation of the cloud's material or condensation of warm and hot interstellar gas (McKee and Ostriker, 1977, Weaver *et al.*, 1977, Begelman and McKee, 1990). As a rule, previous investigations of evaporation of a cloud embedded in hot gas were made in approximation of "thermal wave", which includes effects of thermal conductivity and radiative cooling, but neglects hydrodynamic motions (Zeldovich and Pikelner, 1969, Doroshkevich and Zeldovich, 1981, Balbus and McKee, 1982, Balbus, 1985, McKee and Begelman, 1990). At the same time, it is easy to show that hydrodynamical effects can play an important role in evaporating clouds at least at initial stages of evaporation. This occurs due to pressure excess in outer layers of cloud generated by conductively heated gas, which leads to outflow of gas at outer regions of clouds and to inflow of gas to the cloud's centre. Indeed, the characteristic time of heat transfer from a hot cloud's boundary to its central parts is about $\tau_\kappa \sim \rho R^2/\kappa$, where ρ is the gas density of the cloud, R, its radius, κ (erg K^{-1} cm^{-1} s^{-1}), the thermal conductivity, $\tau_s \sim R/c_s$, the hydrodynamical characteristic time, and c_s is the sound speed in the cloud. When $\tau_\kappa \gg \tau_s$, perturbation of pressure rapidly relaxes over the whole cloud, so that cloud expandes (or evaporates) at nearly constant pressure. But, in the other

cases ($\tau_\kappa \geq \tau_s$ or $\tau_\kappa \leq \tau_s$) dynamical relaxation is as slow as the thermal one, that is, heat transfer is accompanied by the hydrodynamical motions. In this paper we investigate such effects in the evaporating cloud at the initial stages, $t \sim \tau_s$, when hydrodynamical motions are far from steady.

Cowie and McKee (1977), Giuliani (1984), Draine and Giuliani (1984), Böringer and Hartquist (1987) have treated hydrodynamical effects near conductive interfaces separating hot and cold interstellar phases, but they restricted their research to studying the steady outflows of gas from the cloud's boundary. One of the aims of our paper is to demonstrate that the interaction of hot and cold phases at conductive interfaces creates generally two types of coexistent motions: evaporative and implosive modes.

Similar dynamics occurs in a gaseous cloud exposed by heating radiation for which the cloud is optically thick. Absorption of such radiation by outer layers of the cloud creates pressure excess near cloud's edge. Earlier, this problem was investigated for a cloud embedded in H II-zone and compressed by ionizing Ly-c radiation (Dibai and Kaplan, 1964, La Rosa, 1983).

These effects are important for understanding the dynamics of interstellar (Begelman and McKee, 1990, McKee and Begelman, 1990) and intergalactic clouds (Cowie and Songaila, 1977, Shaviv and Salpeter, 1982), and gaseous condensations near quasars (Krolik, et al., 1981). The contraction of gaseous clouds driven by radiation or thermal conductivity is the essential mechanism of global starburst in the framework of the conception of induced star formation (Cammerer and Shchekinov, 1991).

In 2 the hydrodynamical equations with discussion of initial and boundary conditions are given. In 3 the numerical results for the simple form of conductivity and zero cooling rate are discussed. 4 gives the results for zero and nonzero cooling rate, and for thermal conductivity dominated by atoms and/or electrons. The results of radiative-driven implosion of the cloud are discussed in 5, 6 summarizes the principle conclusions.

2. BASIC EQUATIONS

For spherically symmetric flow the master equations in Lagrangian coordinates $dm = \rho r^2 \, dr$ are as follows:

$$\frac{\partial r}{\partial t} = u, \tag{1}$$

$$\frac{\partial}{\partial t}\left(\frac{1}{\rho}\right) = \frac{\partial}{\partial m}(r^2 u), \tag{2}$$

$$\frac{\partial u}{\partial t} = -r^2 \frac{\partial P}{\partial m} - \frac{\partial \phi}{\partial r} + \frac{\partial}{\partial m}(r^2 P_\mu) - \frac{4\mu u}{\rho r^2} - \frac{2(\mu_\theta - \frac{2}{3}\mu)}{r}\frac{\partial(r^2 u)}{\partial m}, \tag{3}$$

$$\frac{\partial E}{\partial t} = -P\frac{\partial(r^2 u)}{\partial m} - \Lambda(T)\rho/m_0^2 + \Gamma/m_0$$

$$+ 2\mu\rho r^4\left(\frac{\partial u}{\partial m}\right)^2 + \frac{4\mu u^2}{\rho r^2} + \left(\mu_\theta - \frac{2}{3}\mu\right)\rho\left(\frac{\partial r^2 u}{\partial m}\right)^2 + \frac{\partial}{\partial m}\left(\kappa\rho r^4 \frac{\partial T}{\partial m}\right), \tag{4}$$

$$E = \frac{P}{(\gamma - 1)\rho}, \tag{15}$$

where u is the radial velocity, ρ is the gas density, P the gaseous pressure, μ the isotropic viscosity, μ_θ the shear viscosity, E the specific energy, $\Lambda(T)$ the cooling function, Γ the heating rate, m_0 the hydrogen mass, κ the thermal conductivity coefficient, T the temperature, $\phi = \phi(r)$ is the gravitational potential,

$$P_\mu = 2\mu\rho r^2 \frac{\partial u}{\partial m} + \left(\mu_\theta - \frac{2}{3}\mu\right)\rho \frac{\partial r^2 u}{\partial m}.$$

In the initial state the cloud with radius R_0, density $\rho_0 (= \text{const})$, and temperature T_0 $(= \text{const})$ is in pressure equilibrium with the intercloud gas with density ρ_h $(= \text{const})$, and temperature $T_h (= \text{const})$: $n_0 T_0 = n_h T_h$, where n is the number density. In our calculation we assume through the article that $T_h = 100 T_0$. The basic dimensional units used in numerical calculation are as follows: R_0, ρ_0 and T_0, so that dimensionless variables are:

$$\tilde{r} = r/R_0, \qquad \tilde{t} = c_{s0}t/R_0, \qquad c_{s0} = (\gamma k T_0/m_0)^{1/2},$$

$$\tilde{u} = u/c_{s0}, \qquad \tilde{\rho} = \rho/\rho_0, \qquad \tilde{P} = P/(k n_0 T_0), \qquad \tilde{\phi} = \phi/c_{s0}^2,$$

$$\tilde{\mu} = \mu/(\rho_0 R_0 c_{s0}), \qquad \tilde{\Lambda} = \Lambda R_0 n_0/(c_{s0}^3 m_0), \qquad \tilde{\Gamma} = \Gamma R_0/(c_{s0}^3 m_0), \tag{6}$$

$$\tilde{\kappa} = \kappa m_0/(k \rho_0 R_0 c_{s0});$$

k is the Boltzman constant; in the following text sign "tilda" will be omitted. Our present calculations are restricted by consideration of non-gravitating clouds, $\phi = 0$. In other words we consider the clouds with an initial ratio of gravitational binding energy to thermal energy sufficiently less unity, but, it is possible that during the advanced contraction of the cloud, this ratio can be reversed. Dynamics of such advanced stages will be described elsewhere (Kovalenko and Shchekinov, 1991).

Three characteristic times determine qualitative features of the investigated problem: hydrodynamical time τ_s, conductive time τ_κ and cooling time τ_c. It should be mentioned, that the description of evaporation in the "thermal wave" approximation permits to parametrize the solution by a single dimensionless number, so called global saturation parameter σ_0, which is equal approximately to the ratio of the free path of atoms (or electrons) in intercloud medium l_h to the radius of a cloud: $\sigma_0 \sim l_h/R_0$ (Cowie and McKee, 1977). In dimensionless form the characteristic times are equal: $\tau_s = 1$, $\tau_\kappa = \kappa^{-1}$, $\tau_c = \Lambda^{-1}$. To exclude the influence of the external boundary computational zone is constructed such that the hydrodynamical time of the external region (hot intercloud gas) τ_s is equal to that of the internal one (cloud's gas) $\tau_s = \tau_{s0}$. It means that the ratio of cell sizes of external to internal regions is $\Delta r_h/\Delta r_0 = c_{sh}/c_{s0} = (T_h/T_0)^{1/2}$ for equal number of cells in these regions: $N_h = N_0$, in numerical calculations we believe $N_h + N_0 = 100$, (subscript "0" belongs to the cloud). It should be noted that characteristic times τ_c and τ_κ depend sharply on gas temperature, so that actually we have the pair of cooling time τ_{c0} and τ_{ch}, and pair of conductive time $\tau_{\kappa0}$ and $\tau_{\kappa h}$. Indeed, near the stable state of atomic interstellar gas $\tau_c \sim \exp(E_{ex}/kT)$, where E_{ex} is the characteristic energy of the "mean" atomic level that provides a cooling of gas. For a quite large contrast of temperature, $T_h/T_0 > 1$, and $kT_0/E_{ex} < 1$ $\tau_{ch} \ll \tau_{c0}$. The ratio of $\tau_{\kappa0}/\tau_{\kappa h}$ for the predominantly neutral gas of cloud with $T_0 = 10^4$ K and hot ionized gas with $T_h = 10^6$ K is about $\tau_{\kappa0}/\tau_{\kappa h} \sim 4 \cdot 10^{-10} T_h^{5/2}/T_0^{1/2} \gg 1$. Moreover, the interrelation between τ_κ and τ_c differs for cloud and intercloud

gas. Indeed, τ_κ and τ_c can be written as follows:

$$\tau_\kappa = \frac{3R_0}{l}\left(\frac{n_0}{n}\right)\frac{c_{s0}}{c_s},$$

and

$$\tau_c \sim \frac{1}{3}\left(\frac{3kT}{2E}\right)\exp\left(\frac{2}{3}\frac{E_{ex}}{kT}\right)\tau_\kappa^{-1},$$

where l is the free path length for the cloud's gas. It is obvious that if the temperature contrast is quite large $T_h/T_0 \gg 1$ there exists a region at conductive interface with

$$\left(\frac{3kT}{2E_x}\right)\exp\left(\frac{2E_{ex}}{3kT}\right) \sim 1,$$

so that in such a region cooling time drops to its minimal value $\tau_c = \tau_c(\text{min}) \sim \tau_\kappa^{-1}$. For clouds with predominantly neutral gas $\tau_\kappa \sim 10^3$ $n_0 R_0(pc) \gg 1$, and $\tau_c(\text{min}) \ll 1$. Thus, there is a hierarchy of characteristic times essential for correct description of the investigated system that differ from one another more than order of magnitude. This means that the matter in question is a typical stiff problem for which especial numerical codes must be used. One of such codes is proposed by Kovalenko (1991): this is an implicit conservative code in Lagrangian variables that conserves mass, energy, and in the absence of dissipation entropy as well. The conservation of entropy means that the effects of scheme viscosity are negligible, and we can regulate the value of dissipation, by entering and varying the coefficients of physical, linear, and/or artificial square viscosity.

3. A SIMPLE MODEL WITH TEMPERATURE-INDEPENDENT CONDUCTIVITY

To investigate the qualitative features of hydrodynamical flow near conductive interfaces, consider a simple case $\kappa = \text{const}$, and $\Lambda = \Gamma = 0$ (Model I). Figure 1 demonstrates the sample $\kappa = 0.01$: in this case thermal perturbation spreads all over small scales $\Delta r \geq \kappa$ and induces almost linear perturbation of hydrodynamical variables. Generally, three flows are created: a focusing compression wave, an outflow of the external layer of cloud, and divergent rarefaction waves. The first two flows are seen clearly in Figure 1a as depressions and peaks in the velocity profiles, the latter is displayed as a dimple on the first velocity profile correspondent to $t = 1/4$. Both the focusing wave and the divergent outflow are excited by a pressure excess in the conductively heated outer layer of the cloud. The rarefaction wave passing from the cloud's boundary outwards is excited by a droop of pressure in intercloud gas near the cloud's boundary due to conductive cooling at the initial time.

The focusing compression wave passes through the cloud in a time $t \sim 1$ becoming more intense due to cumulative factor r^{-2}, and when it reaches the cloud's centre it causes maximal compression of gas, so that density at the centre becomes equal to ~ 2.5. After reflection this perturbation passes in the opposite
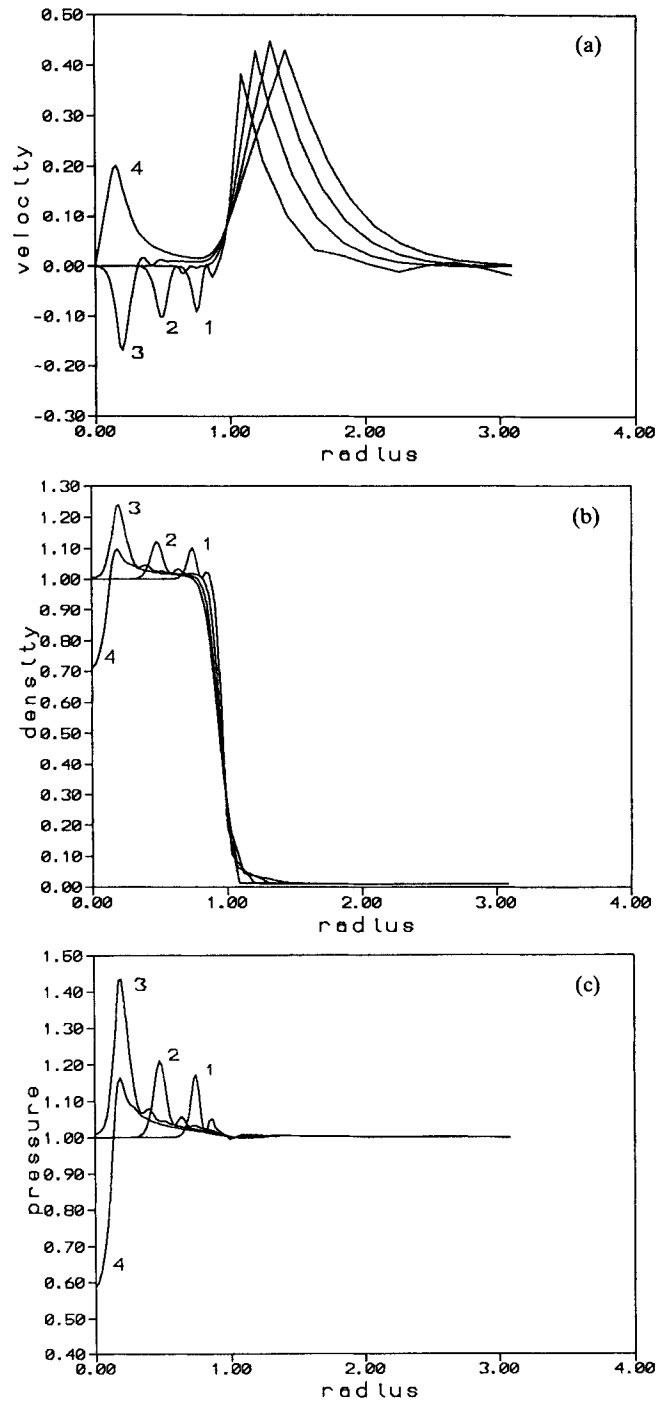
**Figure 1** The profiles of velocity (a), density (b) and pressure (c) in dimensionless units for a cloud embedded in hot gas for a model with temperature independent conductivity, $\kappa = 0.01$, $\mu = 0$. Numbers at the curves correspond to the time interval from the beginning: 1—1/4, 2—1/2, 3—3/4, 4—1 of $t = 1$. Model I.
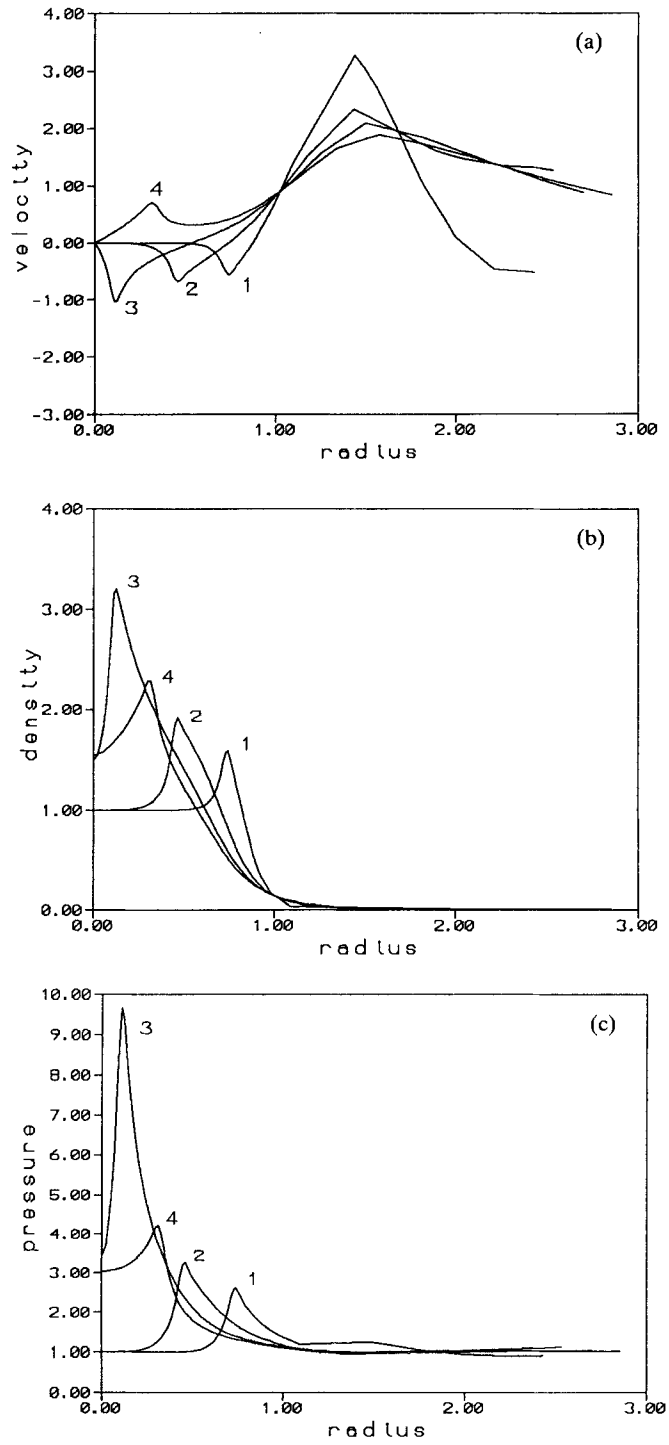
Figure 2 Same as in Figure 1 for $\kappa = 0.1$, $\mu = 0$; $t = 0.7$.

direction as a rarefaction wave (Figures 1b and c). The material flowing out of the cloud's boundary is accelerated at the distance ~0.5 from the boundary by a pressure excess and then it slows down due to collision with environmental gas.

The increase of the conductive coefficient leads to a rise of the magnitude of hydrodynamical perturbation and, as a result, flow becomes essentially nonlinear: amplitude of hydrodynamical variables is in the order of a unit at the beginning. There exists three different regimes of energy transfer dependent on the numerical value of conductivity coefficient: i) linear or almost linear sound waves for $\kappa < T_h^{-1}$; ii) nonlinear flows for $T_h^{-1} < \kappa < 1$, when thermal energy accumulated during a time τ at the beginning in outer layer of cloud of thickness l, is compared with thermal energy of the whole cloud, and characteristic time of
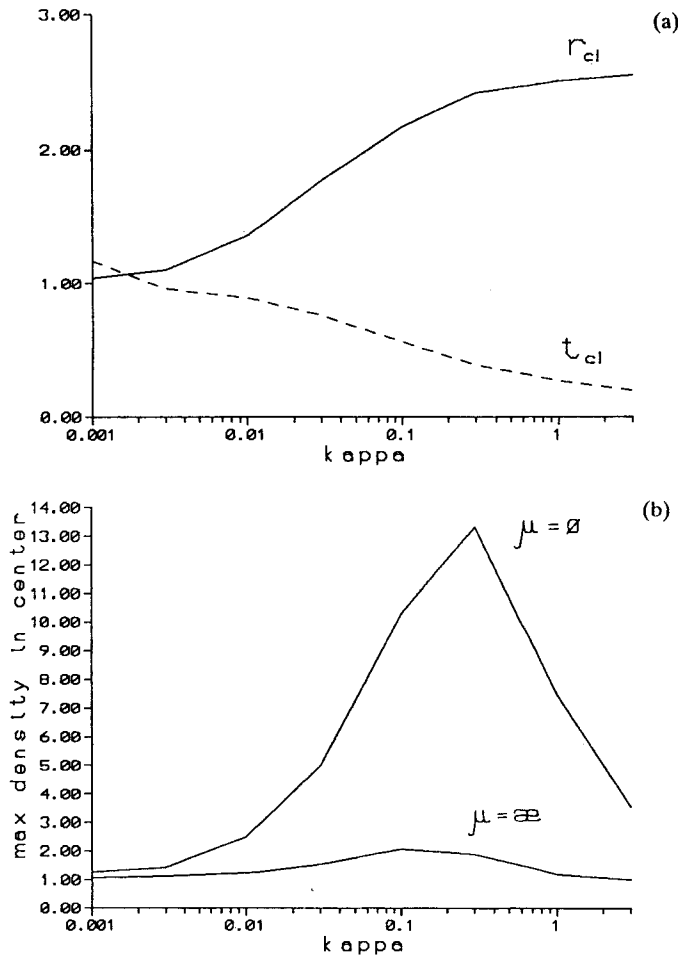
Figure 3 a) The dependence of the time interval needed for a compression wave to reach the clouds centre (dashed) and correspondent radius of the cloud at this moment (solid) on conductivity coefficient, $\mu = 0$. b) The dependence of maximal central density ρ_m on conductivity. Top curve corresponds to $\mu = 0$, bottom one to $\mu = \kappa$.

conductivity is yet larger than the hydrodynamical one; iii) thermal wave passing through the cloud with stimulated comparatively slow hydrodynamical flows spreading all over the cloud for $\kappa > 1$, when the time of conductivity is shorter than the hydrodynamical one. It should be noted, however, that the latter case implies that the atomic free path is larger than the cloud's size, so that the hydrodynamical approach is not yet valid, and all related inferences are of qualitive character. In Figure 2, temporal behaviour of gaseous flow excited by conductivity is plotted for $\kappa = 0.1$. The time interval required for the compression wave to reach the cloud's centre t_m is about half of the hydrodynamical time, and the gas density at this moment is ~ 10, Figure 3. It is a result of the rise of pressure at the outer boundary. But, maximal density at the centre ρ_m caused by the focused compression wave depends on the conductivity coefficient non-monotonically: at $\kappa \sim 0.3$ increasing of ρ_m is replaced by its decreasing (Figure 3b) because the pressure gradient becomes less steep at such κ. On the contrary, the characteristic time t_m is the monotone function of κ, since the raise of κ accelerates the passage of thermal perturbation by both hydrodynamical motion and thermal wave (Figure 3a). A rough estimation gives us $t_m \sim \kappa^{-1/3}$.

It is obvious, that viscous forces smooth gradients of pressure and velocity, so that a hydrodynamical regime becomes softer. As a result, maximal central density ρ_m is a slowly varying function of κ with maximal value only about 2 at $\kappa \sim 0.1$, (lower curve in Figure 3b).

The global kinematic characteristics behave at initial stages very simply: the wave passing through the environmental gas is actually a sound wave with a small amplitude of velocity perturbation. The cloud's boundary and compression wave move with almost constant velocity approximately equal to: $u \sim (\kappa T_h)^{1/3}$.

4. MODELS WITH COOLING AND TEMPERATURE-DEPENDENT CONDUCTIVITY

4.1. *The Case* $\kappa = \kappa_0 T^{1/2}$, $\Lambda = \Gamma = 0$, *(Model II)*.

In predominantly neutral gas, heat transfer is ensured by interatomic collisions with a thermal conductivity coefficient proportional to $T^{1/2}$. Figure 4 demonstrates the dynamics of interaction of cloud's gas with the intercloud gas in this case for $\kappa_0 = 0.01$ and $\mu = \kappa$. There are several differences from the model with $\kappa = \text{const} = 0.01$. Firstly, the time interval for the compression wave to reach the cloud's centre $t_m \sim 0.5$ is approximately half of the corresponded value for $\kappa = 0.01$. It is a result of more effective heat transfer at the cloud's boundary where $\kappa \sim 0.01 T_h^{1/2} = 0.1$ is one order of magnitude larger than in the previous case. Incidently, it provides a larger amplitude of hydrodynamical motions: magnitudes of perturbations of velocity, density and pressure, are about three times higher than in the case with $\kappa = 0.01$. Also, sufficiently larger scales characterize the extension of hydrodynamical perturbation in intercloud gas as it is readily seen in Figure 4a and c. This circumstance is understood to be caused by a large conductivity coefficient in the intercloud medium $\kappa = 0.1$.

On the other hand, the hydrodynamical regime in this case is softer than in the case with $\kappa = \text{const} = 0.1$, because the latter implies a large conductivity coefficient over the whole range including the cold cloud interior.
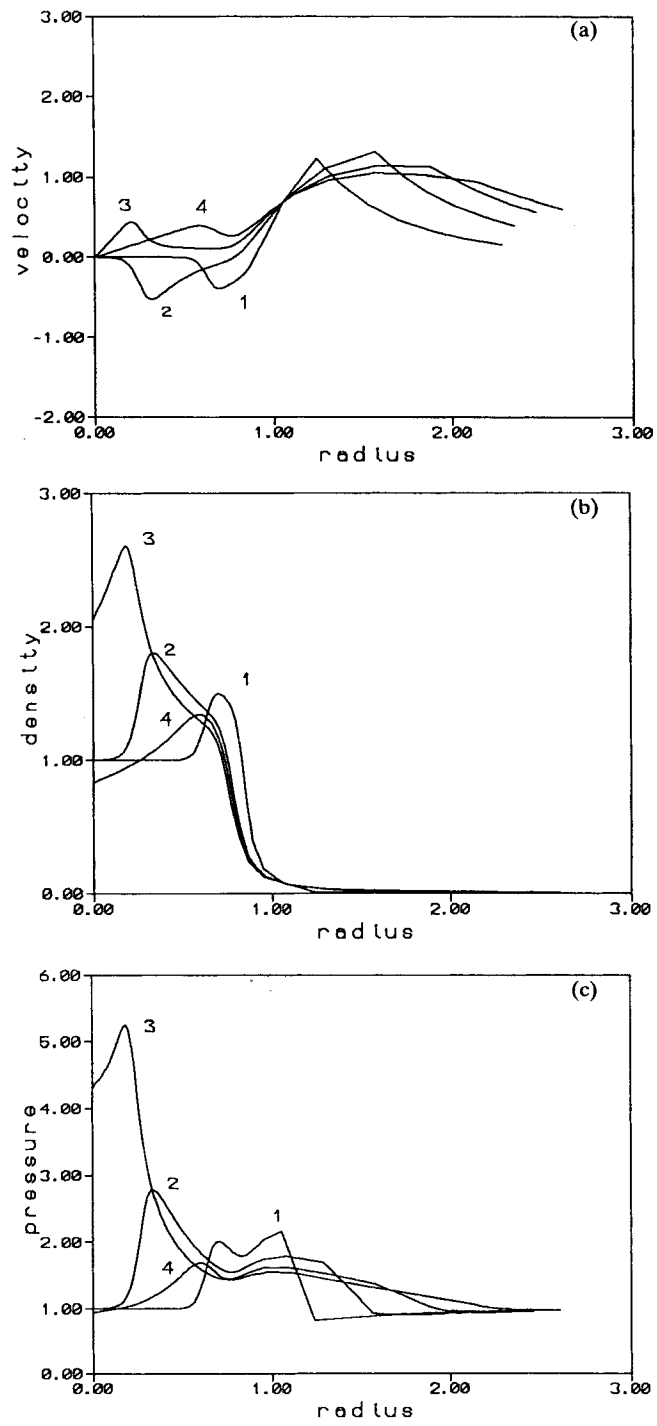
Figure 4 Same as in Figure 1 for temperature-dependent conductivity, $\kappa = \mu = 0.01T^{1/2}$; $t = 1$. Model II.

## 4.2. *Mixed Conductivity*, $\Lambda = \Gamma = 0$, (*Model III*)

The realistic models describing the interaction of warm (10^4 K) and hot ($\sim 10^6$ K) phases of interstellar gas must include both atomic and electronic thermal conductivity, with prevalation of electronic conductivity in hot intercloud gas and at interface separating cloud and intercloud material, and of atomic conductivity in the warm cloud's interior. In Figure 5 hydrodynamical profiles for the model with mixed conductivity $\kappa = \kappa_1 x + \kappa_2 (1 - x)$ and with no heating-cooling processes are plotted. Here $\kappa_1 = \kappa_{10} T^{5/2}$, $\kappa_2 = \kappa_{20} T^{1/2}$, x is a fractional ionization, and $\kappa_{10} = 3 \cdot 10^{-5}$, $\kappa_{20} = 7 \cdot 10^{-4}$, are normalized conductivity coefficients for $T_0 = 10^4$ K, $T_h = 10^6$ K, $R_0 = 1$ pc, $n_0 = 1$ cm^{-3}. Fractional ionization is assumed to be determined by collisional ionization and radiative recombination predominantly of H and He atoms. It causes very steep dependence of x on temperature at the cloud's boundary: $x \sim \exp(-15.8/T)$. It is possible that cosmic ray or X-ray ionization can make this dependence less strong, but in any case qualitative picture remains unchangeable because non-thermal sources are not sufficient to provide prevalence of electronic conductivity at HI temperature $T_0 \leq 10^4$ K.

The most distinctive feature of this model is the formation of an adiabatically heated shell at the cloud boundary pushed by conductivity to the clouds centre with a sharp edge and density contrast ~ 4 far from the centre and with the velocity about $u \sim 5$, so that maximal compression of gas at the centre comes in a time $t_m \sim 0.2$. The maximal density at this moment is about $\rho_m \sim 20$, and pressure $P_m \sim 300$. The outflow wave is localized at the distance ~ 0.5 from the cloud's boundary as in previous cases, but the characteristic size of the region covered by outflow is sufficiently larger, extending to $r \sim 3$ at the beginning, and to $r \sim 5$–6 at $t \sim t_m$. It is a result of a large pressure gradient at the interface. The amplitude of the velocity of outflow wave is readily seen to be several times larger than in the previous model due to the same reason.

4.3. *Mixed Conductivity*, Λ *and* $\Gamma \neq 0$ (*Model IV*)

Let us now consider the dynamics of conductive interaction of the cloud and hot gas in a model with volume heating and cooling. The main properties of such interaction can be described by the simple model that includes the warm ($T = 10^4$ K) HI cloud embedded in hot ($T = 10^6$ K) coronal gas being in pressure equilibrium, without a cold condensed ($T = 10^2$ K) HI core in the central parts of a cloud as assumed in McKee and Ostriker theory (1977). The models with such a central core seem to have the same qualitative properties as those without the core. The reason for such suggestion is that the conductivity coefficient inside the HI cloud, and especially inside the dense core, is determined by atomic collisions. The correspondent conductive-driven hydrodynamical motions have a magnitude sufficiently less than that produced by electron conductivity as is is easily seen from comparison of Figures 4 and 5.

Figure 6 demonstrates the characteristics of flows in a model with radiative heating and cooling for the cloud and environment gas, with parameters accepted in the previous section. The cooling function $\Lambda(T)$ was accepted to be equal to the hydrogenic cooling function, which is parameterizied in dimensionless form as follows: $\Lambda(T) = 2 \ 10^4 (1 + T^{-1}) T^{-1} \exp(-11.8/T)$. In our calculations we believe
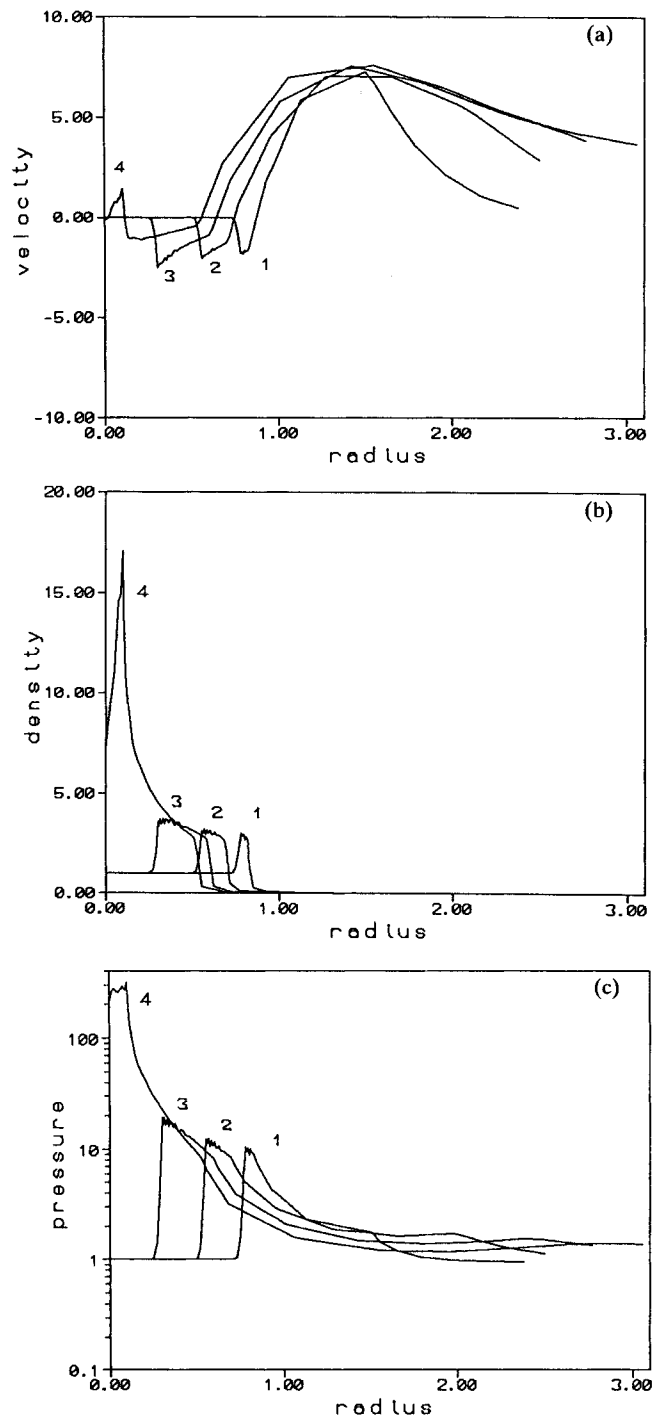
Figure 5 Same as in Figure 1 for temperature-dependent conductivity, $\kappa = 3\,10^{-5} \times T^{5/2} + 7\,10^{-4}(1-x)T^{1/2}$; $t = 0.3$. Model III.
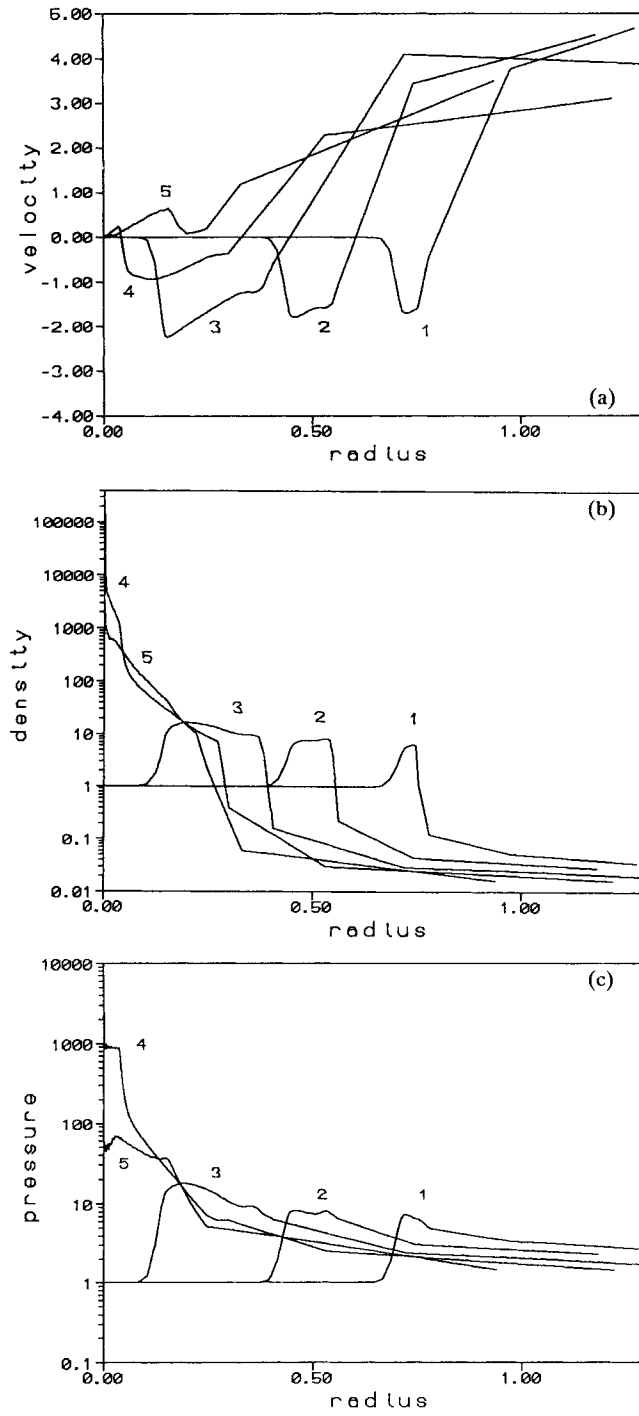
Figure 6 Same as in Figure 5 for the model with cooling; 1—1/8, 2—1/4, 3—3/8, 4—1/2, 5—5/8 of $t = 1$. Model IV.
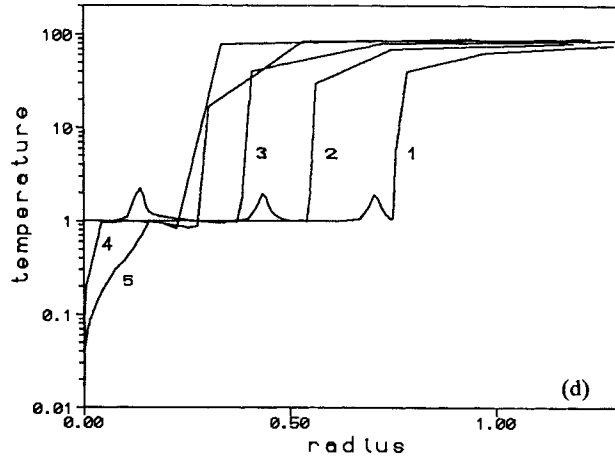
Figure 6 Same as in Figure 5 for the model with cooling; 1—1/8, 2—1/4, 3—3/8, 4—1/2, 5—5/8 of $t = 1$. Model IV.

that the cooling rate is equal to $\Lambda(T)$ n, that is, that cooling is provided by atomic collisions while hydrogenic cooling is really due to excitation of the $2p$ state of H-atoms by electrons. Nevertheless, such approximation reproduces qualitative properties of the cooling rate acceptably. In addition, it gives some perceptible cooling at low temperatures, $T < 1$, thereby making up for the lack of heavy elements to a certain extent. The heating rate was assumed to be balanced by the cooling of the cloud's gas with $n_0 = 1$ and $T_0 = 1$, so that $\Gamma \simeq 0.3$. This means, particularly, that the hot coronal gas being in pressure equilibrium with the cloud's gas is dominated by cooling because its cooling rate $\Lambda(T_h)n_h \sim 2 > \Gamma$. This results in a slow decrease of hot gas temperature: approximately 10% during a time $t = 1$, Figure 6d.

There are several important differences in this model from the previous one. Firstly, the characteristic time of focusing of the compression flow $t_m = 0.42$ is sufficiently larger than in the model without radiative cooling. This difference can be understood in terms of the decreasing of characteristic hydrodynamical velocity $u = (\gamma P / \rho)^{1/2}$ which droops in the radiative model due to the sharp raise in density of compressed gas (Figure 6b). At the same time the amplitudes of velocities both for the compression and outflow waves are approximately the same as in the previous case. At the cloud boundary, a warm and dense shell is formed as in the previous model, but quite more massive. As a result, the pressure and density at the cloud's centre are sufficiently larger when the compression wave reaches it: $P \sim 10^3$ and $\rho \sim 10^4$ respectively. Such a compression provides efficient cooling of the gas, so that the central temperature falls down to 0.07. This decrease is caused by our assumption on the independence of cooling rate on fractional ionization, and as mentioned above can reproduce partly the properties of a real cloud's dynamics with heavy elements cooling.

The gas of the dense shell cools down to $T \sim 1$ due to radiative losses that dominate conductive heating because the exponential factor of the cooling function $\Lambda(T) \sim \exp(-11.8/T)$ is less steep than that of fractional ionization
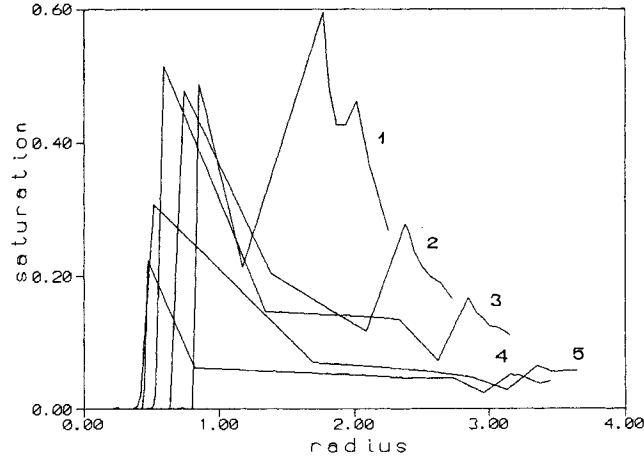
Figure 7 The profiles of the local saturation parameter σ_T for the model IVm.

$x(T) \sim \exp(-15.8/T)$. But, at the leading edge of the compression wave (nearer to the clouds centre) some increase of temperature due to adiabatic heating takes place, Figure 6d.

To control whether heat transfer is saturated in this model, we investigated the problem with modified heat transfer equation (Model IVm) using the approximation of the effective coefficient of thermal conductivity given by Balbus and McKee (1982) and Giuliani (1984): $\kappa_e = \kappa/(1 + \sigma_T)$, where $\sigma_T \equiv |\kappa\nabla T|/q_{sat}$, is local saturation parameter, $q_{sat} = 5\rho(kT/m_0)^{3/2}$. The profiles of $\sigma_T(r, t)$ are plotted in Figure 7. The maximal value of $\sigma_T \approx 0.5$ is reached at the cloud's boundary where the differences of the temperature in neighbouring layers are the largest. However, generally, local saturation parameter is of sufficiently less unity and, as a result, the differences between models IV and IVm are negligible, so that hydrodynamical profiles are practically the same as in Figure 6. It is obvious, that the previous models with $\Lambda = \Gamma = 0$ are also unsaturated because a gas cooling increases the temperature gradients.

5. RADIATIVE-DRIVEN IMPLOSION

Earlier, the problem of photo-implosion of interstellar clouds was solved by Dibai and Kaplan (1964), and La Rosa (1983). Their study included the dynamics of clouds exposed to ultraviolet ionizing radiation of the Lyman continuum: ionizing photons absorbed by the outer layer of a cloud generate an excess of pressure and drive ionization and shock fronts to the clouds centre. Such consideration necessarily describes the properties of clouds localized inside HII regions in the vicinity of OB stars. However, similar effects may take place in diffuse interstellar matter outside HII-zones as well. Indeed, the heating radiation (X-rays, cosmic rays or UV photons beyond the Lyman limit) exposing an opaque cloud is absorbed by its outer layer of optical depth equal to about $\tau \sim 1$–3, and thereby the efficiency of heating drops on a length of absorption. As a consequence, the

pressure gradient rises and pushes the gas to the cloud's centre. Thus, such effect must be important for interstellar clouds with a column density of $N(H) \geq 10^{21}\,\text{cm}^{-2}$. In particular, the diffuse clouds with $n_0 \sim 10^2\,\text{cm}^{-3}$ and $R_0 > 3\,\text{pc}$ are readily seen to be subjected to such influence of interstellar radiation.

In this paragraph we describe the model that includes a cold cloud $(T_0 = 10^2\,\text{K})$ embedded in warm interstellar gas $(T_h = 10^4\,\text{K})$ initially being in pressure equilibrium. In the initial state both cloud and intercloud gas are believed to be in a heating—cooling balance, with the thermal state being described by the equation $\Lambda(T)n = \Gamma$ with an equal heating rate through the cloud and intercloud medium. This means that the cloud's gas is transparent for heating radiation, and such assumption implies a quite limited class of agents, which are able to satisfy these conditions. For example, X-ray photons will penetrate a cloud if their energy is quite large:

$$E_X > 40(n_0/10^3\,\text{cm}^{-3})^{2/5}(R_0/1\,\text{pc})^{2/5}Ry. \tag{7}$$

Actually, heating mechanisms seem to be different for cloud and intercloud gas, but in our model aimed at the investigation of the qualitative features of radiative-driven implosion of clouds such an assumption is quite pertinent. To be specific, we accept that initial thermal equilibrium is maintained by X-rays with sufficiently large energy $(7):\Gamma = \Gamma(X)$. In Figure 8 the conventional (P, ρ) diagrams are plotted for interstellar gas in thermal balance. The bottom curve corresponds to the initial (unperturbed) equation of state.

At the time $t = 0$ the intercloud medium is filled suddenly by UV-radiation beyond the Lyman limit, for which the cloud is opaque. Electrons ejected by UV-photons from the surfaces of dust grains heat the gas. As a result, the heating rate becomes equal to the sum $\Gamma + \Gamma(UV)$, and the $P(\rho)$ curve is shifted to the
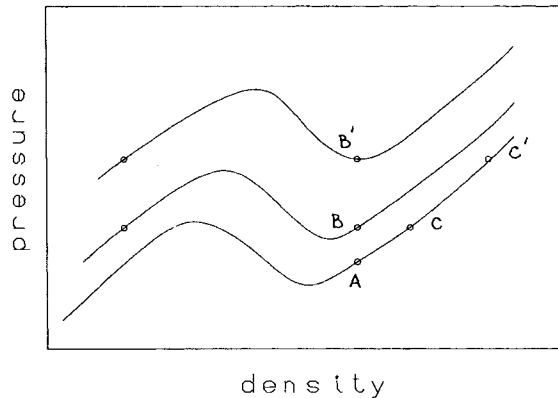

density

Figure 8 (P, ρ) diagram. Point A corresponds to the initial state of the cloud's equilibrium, B–to the state of the optically thin cloud with an increased heating rate and with pressure that corresponds to a constant density of intercloud gas, C–to the state of the optically thick cloud supported by increased external pressure. Points at left parts of $P(\rho)$ curves correspond to intercloud pressure with constant density of intercloud gas. Points B' and C' are the same as B and C for extremely high additional heating rates. This scheme is valid until intercloud density is constant. After intercloud pressure relaxes to the external one, points B, C and C' shift to lower parts of the curves. But, such relaxation takes place in a time equal to the hydrodynamical characteristic time of interstellar gas as a whole.

top-right as shown in Figure 8, so that if a cloud would be transparent to the UV-photons it must be compressed or expanded depending on whether the intercloud pressure rises sufficiently or not. However, in our case UV-radiation is absorbed by the outer layer of cloud where properties of gas correspond to a new equation of state, and in the cloud's interior, the former unperturbed heating rate determines the state of gas, which has to be more dense to balance pressure excess near the cloud's boundary.
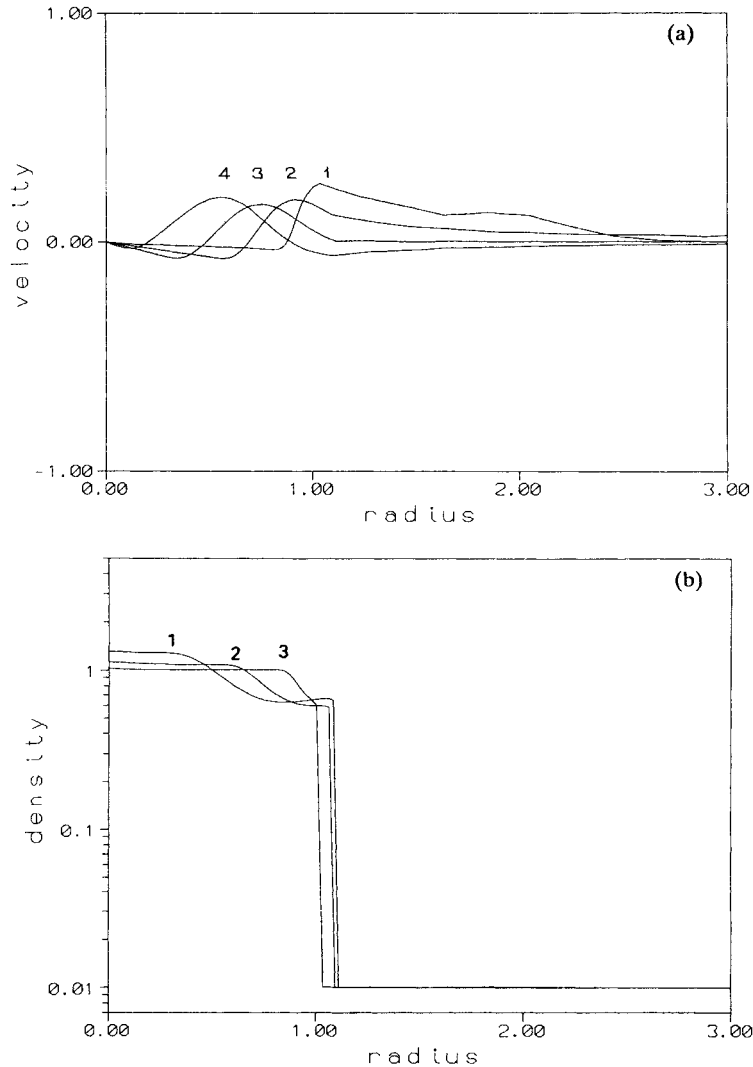

Figure 9 Dynamics of the cloud exposed by additional heating with a relative heating rate $g = 1$; total optical depth of the cloud to the additional heating radiation is $\tau(0) = 1.67$; 1—3/20, 2—9/20, 3—15/20, 4—21/20 of $t = 1.2$.

In our numerical calculation we describe the total heating rate of interstellar gas by the equation $\Gamma = \Gamma_0(1 + g)$, where Γ_0 corresponds to the unperturbed state, and factor g is the relative heating rate by UV-radiation. Consequently, the cloud's gas is heated with total rate $\Gamma(r) = \Gamma_0[1 + g \exp(-\tau(r))]$, where $\tau(r)$ is the optical depth of the outer layer of cloud with a thickness of $R_0 - r$ to the UV heating radiation. We believe optical depth to be determined by dust extinction with the cross-section $\sigma = 10^{-21}\,\mathrm{cm}^2$, so that $\tau(r) = \sigma \int_r^{R_0} n(r)\,dr$. Numerical
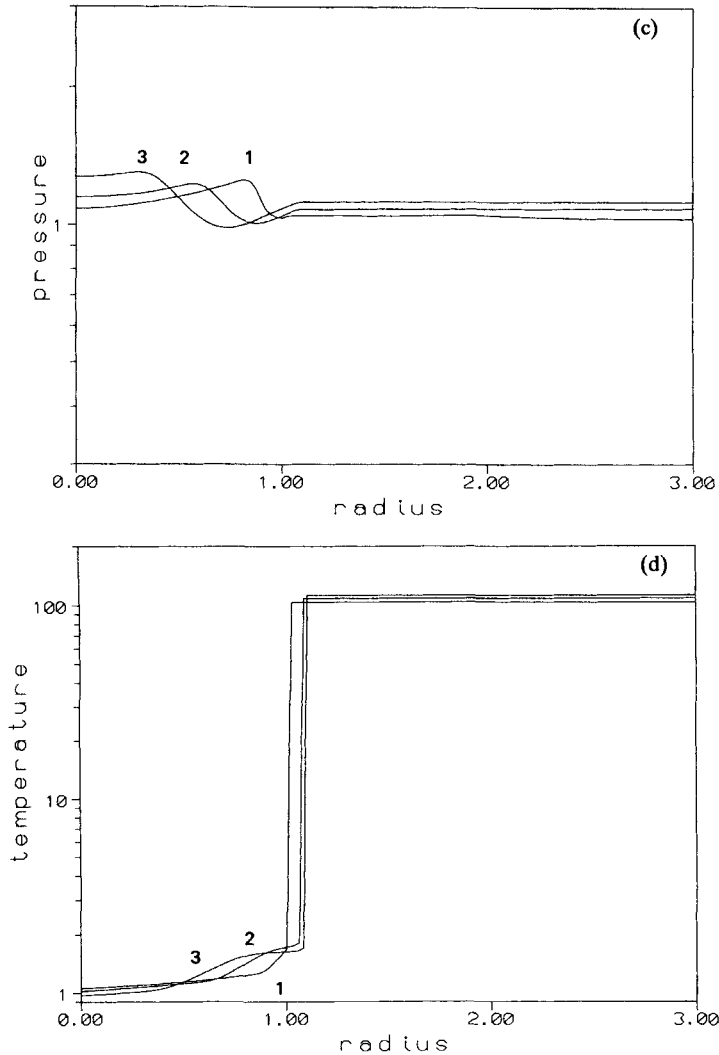
Figure 9 Dynamics of the cloud exposed by additional heating with a relative heating rate $g = 1$; total optical depth of the cloud to the additional heating radiation is $\tau(0) = 1.67$; 1—3/20, 2—9/20, 3—15/20, 4—21/20 of $t = 1.2$.

values of heating and cooling rates were accepted as follows: $\Gamma_0 = 4.5\,10^{-25}\,\text{erg/s}$, and $\Lambda(T) = 2.2\,10^{-24}(1 + 8.2\,10^{-3}(T-5000)^3)\,\text{erg cm}^3/\text{s}$, the latter reproduces the qualitative form of the interstellar cooling function; the thermal conductivity is believed to be zero. Figure 9 demonstrates the temporal behaviour of a cloud of radius $R_0 = 5.32\,\text{pc}$ exposed by UV-flux with $g = 1$. The initial total optical depth to the UV is $\tau(0) = 1.67$. It is easy to see that the excess of pressure near the cloud's boundary pushes a compression wave to the centre, so that in a time of $t_m \sim 1$ central regions of cloud are approximately twofold denser. On the other hand, a negative pressure gradient at the outer parts of the absorbing layer drives
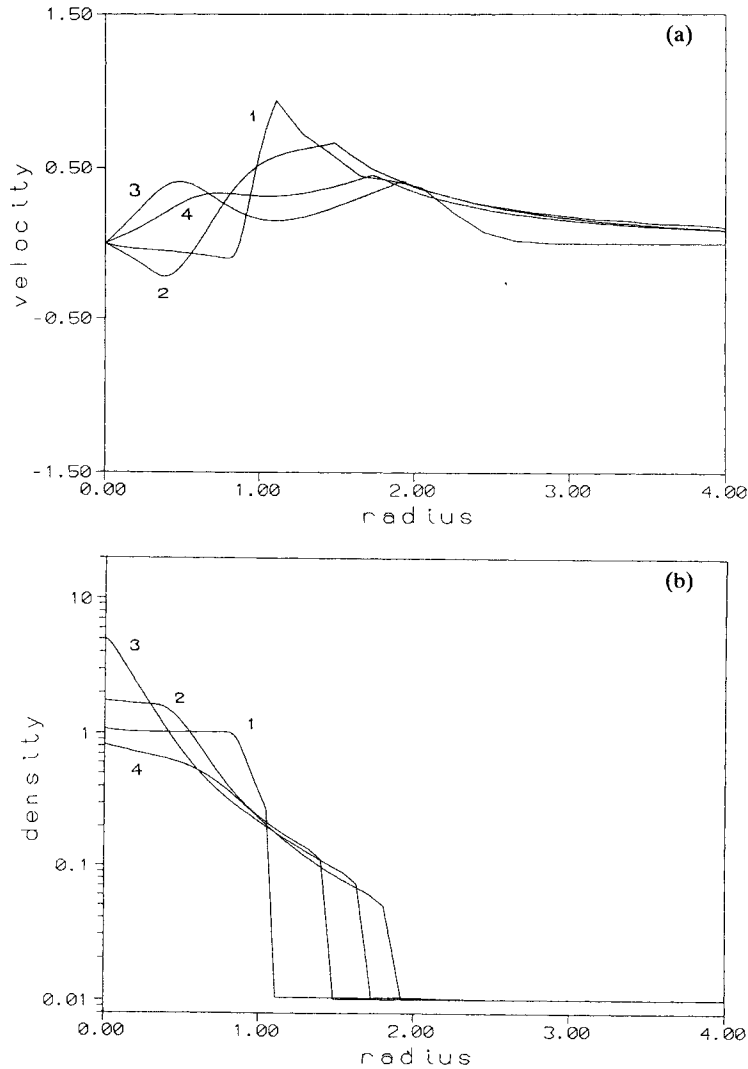
Figure 10   Same as in Figure 9 for $g = 3$. 1—3/20, 2—12/20, 3—21/20, 4—30/20 of $t = 1$.

the rarefaction wave out of the cloud. The final state of a cloud is expected to be the new equalibrium state as demonstrated by (P, ρ) diagram, Figure 8.

Another model with $g = 3$ is plotted in Figure 10. On the (P, ρ) diagram this model corresponds to the top curve, which illustrates the phase equilibrium of gas heated by an extremely high heating rate, when the clouds phase cannot be maintained by intercloud pressure. There are some interesting details in this model. At the initial stage, the pressure profile has three characteristic parts: the inner part with positive pressure gradient, outer layer of cloud, and neighbouring layer of intercloud gas with negative pressure gradient (curve 1 in Figure 10c).
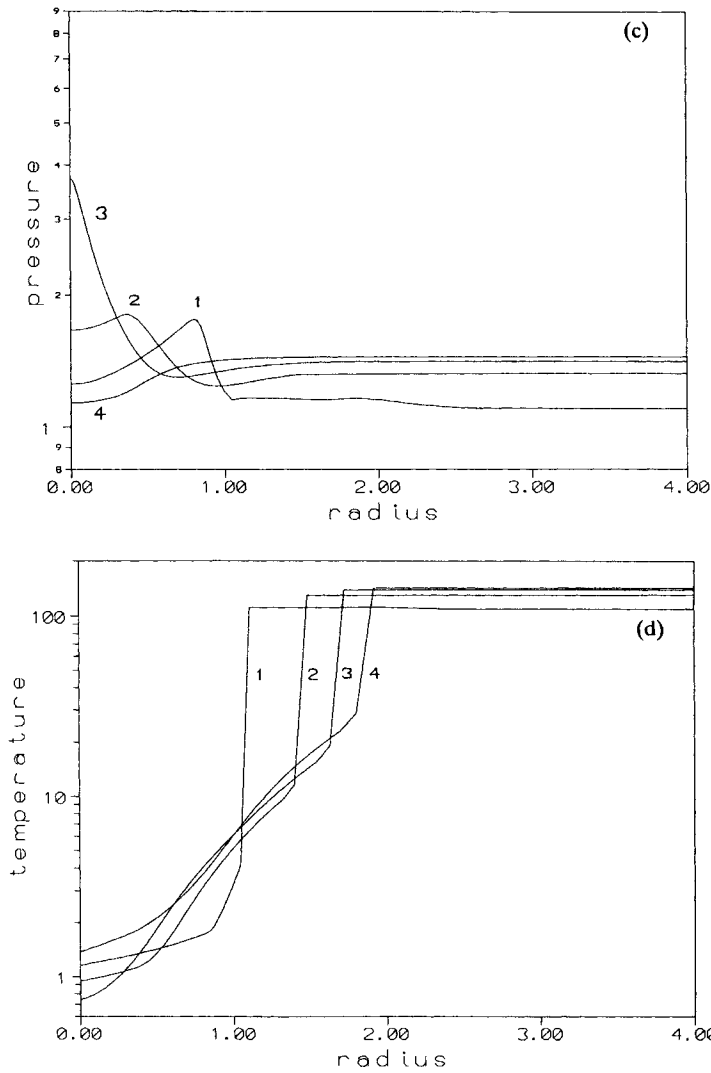
Figure 10 Same as in Figure 9 for $g = 3$. 1—3/20, 2—12/20, 3—21/20, 4—30/20 of $t = 1$.

The latter is caused by adiabatical heating of intercloud gas pushed initially by the expanded cloud, and due to the high mobility of the intercloud gas, it provides quite a developed motion near the outside of the cloud, but later this motion is dumped. The outer negative pressure gradient is approximately constant during a time $t = 1$. It results in the decrease of velocity amplitude of the rarefaction wave because the mass of the outer layers of cloud driven by this pressure rises. The maximal compression of gas at the centre, $\rho_m \sim 4$, is larger than in the previous case because of more intense UV-heating at the cloud's boundary. Intercloud pressure is naturally raised due to additional heating, but the cloud's interior
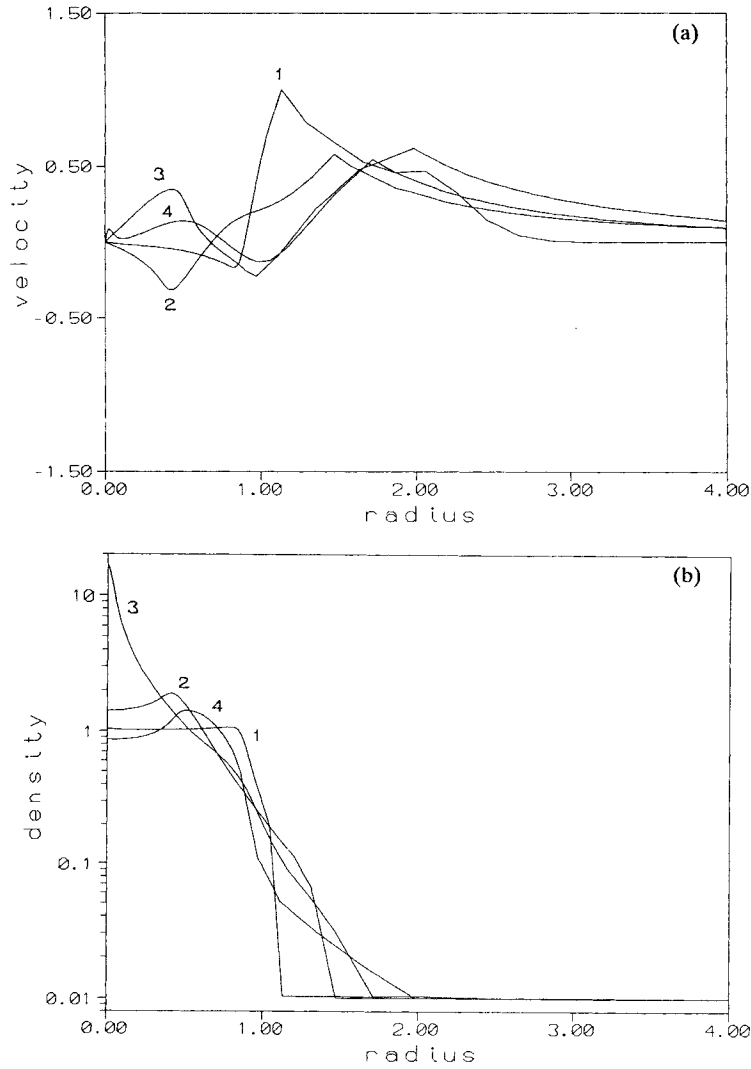
Figure 11   Same as in Figure 9 for $\tau(0) = 3.34$, and $g = 3$; a), b) and c): 1—3/20, 2—12/20, 3—21/20, 4—30/20 of $t = 1.2$ d): 1—1/20, 2—7/20, 3—17/20 of t.

compression is obviously caused mainly by the effects connected with absorption of UV radiation at the boundary. Unlike the previous case, the dynamics of the final stages of the cloud in the model with large UV-heating are expected to be correspondent to a smoothing with intercloud gas (point E in $P(\rho)$ curve) unless gravitational forces prevent it (Kovalenko and Shchekinov, 1991).

The dynamical effects of absorption of heating radiation are obviously increased as the radius of a cloud increases. For instance, maximal density at the centre is about 3 in a model with initial optical depth $\tau(0) = 3.34$ and $g = 1$. Cumulative motions are still more intense in a model with $g = 3$. In Figure 11 the
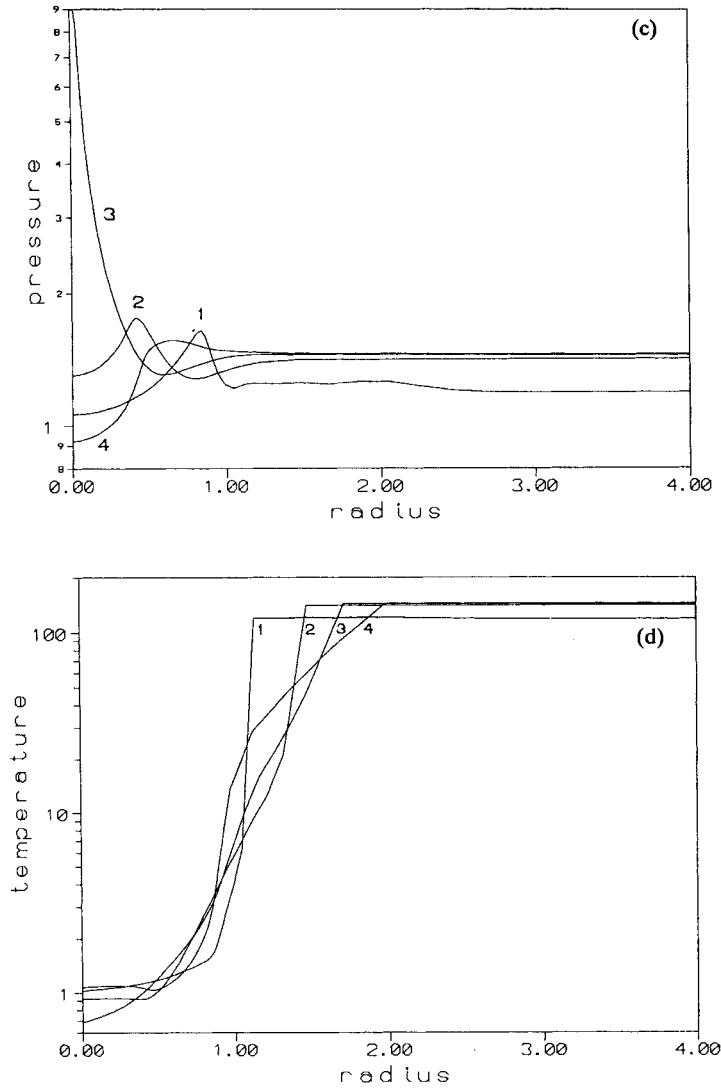
Figure 11   Same as in Figure 9 for $\tau(0) = 3.34$, and $g = 3$; a), b) and c): 1—3/20, 2—12/20, 3—21/20, 4—30/20 of $t = 1.2$ d): 1—1/20, 2—7/20, 3—17/20 of t.

characteristic profiles are plotted for this case. While being qualitatively similar to the previous model, gaseous flow is characterized by larger magnitudes of hydrodynamical variables, especially in the central parts. Particularly, the maximal density at the centre is $\rho_m = 20$.

6. CONCLUSIONS

The above consideration allows us to conclude that the general feature of the hydrodynamics of a gaseous cloud subjected to the influence of hot surrounding gas, or absorbed heating radiation, is the coexistence of two kinds of flows: expansion of the outer layers of cloud, and compression of its inner parts. Such conclusion has an important consequence for interstellar gas physics. Firstly, it means that conductive interfaces separating hot gas from cold clouds, and absorbing interstellar UV radiation as well, can develop extremely high pressure in a cloud's gas being initially in pressure equilibrium with the intercloud environment. It is possible that this mechanism is able to provide an enhanced star formation rate in the regions of interstellar medium with a large filling factor of coronal gas, or with a high intensity of UV radiation (or low-energy cosmic rays and soft X-rays for which clouds are opaque). Secondly, additional compression of clouds by hot environments causes an increasing rate of radiative losses, and therefore, additional heating sources can be required for interstellar gas to be thermally balanced as a whole, These problems will be considered in detail in the following paper (Kovalenko and Shchekinov, 1991).

One of the interesting consequences of the above consideration is that the outflowing gas of an evaporating cloud has a characteristic velocity about 5–7 larger than sound speed of cloud's gas, (see Figures 5 and 6), that is, in dimensional units about 50–70 km/s. This means that Doppler width of absorption lines of highly-charged ions (NV, OVI, etc) formed in conductive interfaces are too large to be detected by Copernicus spectrometer, and as a consequence the numerous evaporating HI-cloudlets floating in coronal gas are apparently not able to ensure the observable properties of highly-charged ions completely, as proposed by McKee and Ostriker (1977).

As mentioned above, an extremal increase of pressure and density (over three and four orders of magnitude, respectively, in the model with cooling, Figure 6) is connected partly with the cumulative factor r^{-2}. Actually this factor is weakened because of lack of exact spherical symmetry, but the general ability of conductive interfaces (or absorbed heating radiation) to generate a compression wave with sufficiently large amplitude (at least 10–20 times of unperturbed one) is undoubtedly independent of geometry.

ACKNOWLEDGEMENTS

The majority of our results were obtained during our stay at the Tartu Astrophysical Observatory. We are grateful to U. Haud, E. Saar and T. Viik for their cordiality. We also appreciate the assistance of E. Kasak in providing an opportunity to use the computer facilities of the Tartu Astrophysical Observatory. Useful discussion with V. I. Korchagin and A. D. Ryabtsev are gratefully acknowledged. Finally, we are indebted to Diana Swander for careful reading of the manuscript and improvement of the text.

References

Balbus, S. A. (1985). Classical thermal evaporation of clouds: an electrostatic analogy. *Astrophys. J.*, **291**, 518–522.

Balbus, S. A. and McKee, C. (1982). The evaporation of spherical clouds in a hot gas. III. Suprathermal evaporation. *Astrophys. J.*, **252**, 529–552.

Begelman, M. and McKee, C. (1990). Global effects of thermal conduction on two-phase media. *Astrophys. J.*, **358**, 375–391.

Böhringer, H. and Hartquist, T. W. (1987). Steady models of radiatively modified conductively driven evaporation from interstellar clouds. *Monthly Notic. Roy. Astron. Soc.*, **228**, 915–931.

Cammerer, M. and Shchekinov, Yu. (1991). Long-range forces in induced star formation. *Astron. and Astrophys*, in press.

Cowie, L. L. and McKee, C. (1977). The evaporation of spherical clouds in a hot gas. I. Classical and saturated mass loss rate. *Astrophys. J.*, **211**, 135–146.

Cowie, L. L. and Songaila, A. (1977). Thermal evaporation of gas within galaxies by a hot intergalactic medium. *Nature*, **266**, 501–503.

Dibai, E. A. and Kaplan, S. A. (1964). Cumulative shock waves in interstellar medium. *Astron. Zh.*, **41**, 652–656.

Doroshkevich, A. G. and Zeldovich, Ya. B. (1981). *ZhETF*, **80**, 801.

Draine, B. T. and Giuliani, J. L., Jr. (1984). Thermal evaporation of spherical clouds: effects of viscous stresses, *Astrophys. J.*, **281**, 690–701.

Giuliani, J. L., Jr. (1984). On the dynamics of evaporating cloud envelopes. *Astrophys. J.*, **277**, 605–614.

Kovalenko, I. (1991). Superconservative difference scheme for gas dynamics, in preparation.

Kovalenko, I. and Shchekinov, Yu. (1991). Heat- and radiative-driven implosion of interstellar clouds. II. Advanced dynamics. *Astron. and Astrophys. Trans.*, in preparation.

Krolik, J. H., McKee, C. and Tarter, C. (1981). Two-phase models of quasar emission line regions. *Astrophys. J.*, **249**, 422–442.

La Rosa, T. N. (1983). Radiatively induced star formation. *Astrophys. J.*, **274**, 815–821.

McKee, C. and Ostriker, J. (1977). A theory of the interstellar medium: three components regulated by supernova explosions in inhomogeneous substrate. *Astrophys. J.*, **218**, 148–169.

McKee, C. and Begelman, M. C. (1990). Steady evaporation and condensation of isolated clouds in hot plasma. *Astrophys. J.*, **358**, 392–398.

Shaviv, G. and Salpeter, E. E. (1982). Gas dynamics of flow past galaxies. *Astron. and Astrophys.*, **110**, 300–315.

Weaver, R., McCray, R., Castor, J., Shapiro, P. and Moore, R. (1977). Interstellar bubbles. II. Structure and evolution. *Astrophys. J.*, **218**, 377–395.

Zeldovich, Ya. B. and Pikelner, S. B. (1969). *Journ. Experim. and Theor. Phys.*, **29**, 170.